IJCRT.ORG ISSN : 2320-2882

INTERNATIONAL JOURNAL OF CREATIVE RESEARCH THOUGHTS (IJCRT)

An International Open Access, Peer-reviewed, Refereed Journal

# A REVIEW OF DIFFERENT COMPENSATION TECHNIQUES FOR WIRELESS POWER TRANSFER TOPOLOGIES

**[1]Indranil Kushary, [2]Avijit Chakraborty, [3]Subinoy Sarkar**

[1]Lecturer , [2]Associate Professor, [3]Lecturer

[1]Electrical Engineering,

[1]Technique Polytechnic Institute, Hooghly, India

***Abstract:*** Wireless power transfer (WPT) stands as a cutting-edge technology facilitating electricity transmission across distances sans physical contact. It presents substantial advantages for modern automation systems, medical applications, consumer electronics, and more. This comprehensive review delves into existing compensation topologies specifically designed for the loosely coupled transformer. It meticulously evaluates these topologies based on their fundamental and advanced functions. This paper scrutinizes individual passive resonant networks deployed to maintain a constant (load-independent) voltage or current output, providing a detailed analysis and summarization. Furthermore, it showcases popular compensation topologies in WPT as practical examples, showcasing how they amalgamate multiple blocks of resonant networks. The study also includes analyses concerning input zero phase angle (ZPA) and soft-switching. This paper focuses into the discussion of compensation requisites essential for achieving maximum efficiency across diverse WPT application areas. It explores how various application contexts necessitate distinct compensation strategies to optimize efficiency.

***Index Terms*** **- Wireless power transfer, Softswitching.**

Introduction: -For over a century, engineers have envisioned the transmission of electrical power through the air, a concept stemming from Faraday's law of induction. Shortly after this principle's proposal, the notion of wireless or inductive power transfer emerged. Nikola Tesla, a pioneering figure in this field during the 1910s, ambitiously proposed the use of his Wardenclyffe Tower to transmit substantial amounts of electrical power globally. While Tesla's approach was deemed impractical and ultimately unsuccessful, his enduring legacy in advancing wireless energy transmission remains significant.

In the contemporary era, wireless power transfer has burgeoned into a global commercial industry valued at $1 billion [5]. This cutting-edge technology has been applied in diverse areas, ranging from charging household devices like electric toothbrushes to facilitating wireless charging for mobile phones through dedicated platforms [6-13]. Additionally, it has found significant use in the medical field, providing wireless power to implantable devices [14-20]. Expanding its reach, medium- to high-power applications now involve continuous power transfer for people movers [21, 22], contactless battery charging for moving actuators [23, 24], and electric vehicles (EVs) [25-36].

To enable power transfer without physical contact, a loosely coupled transformer with a substantial separation between the primary and secondary windings is indispensable. This considerable winding separation results in a relatively large leakage inductance, heightened proximity-effect, and increased winding resistances.

Additionally, the magnetizing flux experiences a significant reduction, leading to lower magnetizing inductance and mutual inductance.

For coils within a Wireless Power Transfer (WPT) system operating at a frequency well below their self-resonant frequencies (SRF) [37], the incorporation of additional compensation capacitors becomes necessary to establish resonant tanks on both the primary and secondary sides. While earlier wireless circuit designs featured single-sided compensation [19, 38], this approach has been superseded by double-sided compensation. The shift is attributed to the limitations of single-sided compensation, which offers fewer adjustable resonant parameters, thereby failing to provide sufficient degrees of freedom to meet all WPT system design criteria. This paper conducts a comprehensive review, comparison, and evaluation of compensation topologies for WPT systems and their applications.

"COMPENSATION REQUIREMENTS

1) Optimization of VA Rating and Enhancement of Power Transfer Efficiency

The fundamental necessity for a compensation capacitor lies in its ability to resonate with the primary and/or secondary inductance, thereby supplying the reactive power required for the inductances to generate a sufficient magnetic field [39]. Consequently, for the primary coil of a loosely coupled transformer, the primary function of compensation is to minimize the input apparent power or, in other words, minimize the VA rating of the power supply [28, 40, 41]. On the secondary side, compensation serves to neutralize the inductance of the secondary coil, aiming to maximize transfer capability [29, 42, 43].

2) Maintenance of Constant Voltage or Current Output

A Wireless Power Transfer (WPT) system involves numerous parameters that may undergo changes during operation. For instance, in a transcutaneous energy transmission system (TETS), the air gap fluctuates in real-time as the patient breathes [44, 45]. In a roadway vehicle inductive power transfer (IPT) system, the number of loads may vary during charging [5, 25, 29]. Consequently, effective controllability is a desirable feature for a WPT system to adapt to parameter variations. Meanwhile, the compensation topology can be chosen to achieve a constant (or load-independent) current or constant-voltage output without the need for a control circuit. This proves advantageous in ensuring robust controllability."

3) Maximizing Efficiency

As indicated in [46, 47], the highest attainable efficiency of a Wireless Power Transfer (WPT) system is determined by two critical parameters: the coupling coefficient and the quality factors of the windings. However, to realize this maximum efficiency, adequate compensation becomes imperative. Achieving high efficiency is also contingent upon incorporating soft-switching techniques. Typically, a half-bridge or full-bridge converter is employed for modulating a DC voltage to drive the resonant circuit. When MOSFETs serve as the switching components, the converter can capitalize on turn-on zero voltage switching (ZVS) by operating above resonance, where the resonant-tank current lags the voltage modulated by the active switches [48]. As the input phase angle can be adjusted through the value of compensation capacitors, the selection of compensation should also prioritize considerations for soft-switching.

4) Resilience to Bifurcation and Other Characteristics

The bifurcation phenomenon in a WPT system occurs when the frequency required to achieve zero phase angle (ZPA) is not unique [40, 49]. The number of frequency points for ZPA is linked to the loading condition, compensation topologies, and capacitor values. To ensure system stability, it is crucial to avoid this bifurcation phenomenon, particularly when dealing with multiple loading scenarios and variable frequency control. Other essential features, including insensitivity to parameter changes and suitability for bi-directional power flow, should also be taken into account for specific applications. Evaluation of compensation topologies should be conducted based on the aforementioned compensation objectives, considering their applications and anticipated operations. The subsequent sections delve into some of the key features mentioned above, along with discussions on various compensation topologies."

## III. PRINCIPLES OF CONSTANT-VOLTAGE OR CONSTANT-CURRENT OUTPUT

This section explores the methodologies for achieving a constant-current or constant-voltage output through resonant circuits. The constant-current or constant-voltage output achieved by a resonant network implies that the voltage or current magnitude (UOUT or IOUT) across the loading resistance RL remains independent of the value of RL, giving the resonant network characteristics akin to those of a voltage or current source.

In the analysis of Wireless Power Transfer (WPT) resonant circuits, the assumption of a frequency-domain equivalent circuit is a standard practice, where only the fundamental component is considered for simplicity [12, 28, 40, 50, 51]. Although the fundamental component approximation is a straightforward analysis method that typically provides sufficient accuracy for a high-quality factor resonant circuit operating near resonance, it may introduce some error due to the switching components of an H-bridge inverter and rectifier. Consequently, for a more accurate study, such as investigating zero current switching (ZCS) requirements (the accurate primary current during switching on), consideration of higher-order harmonics becomes necessary [49]. In this paper, we exclusively utilize the fundamental component to analyze the resonant network characteristics."

The schematic of a passive resonant network is illustrated in Fig. 1. The power source may be either a voltage source or a current source. To ensure that the output voltage amplitude remains independent of the RL value, the choice of configuration for the passive resonant network is contingent on the type of power source employed. When utilizing a voltage power source, achieving a constant-voltage output requires adopting a T-circuit configuration, as depicted in Fig. 2 (a)

The T-circuit in Fig. 2(a) has equations

$U_{OUT} = I_{OUT} * R_L$

$U_{IN} = I_{IN} * Z_1 + (I_{IN} - I_{OUT}) Z_3$ (1)

$U_{IN} = I_{IN} * Z_1 + I_{OUT} * Z_2 + U_{OUT}$

The relationship between the input voltage $U_{IN}$ and the output voltage $U_{OUT}$ can be derived as

$$U_{in} = \left(1 + \frac{z_1}{z_3}\right) U_{out} + \frac{\Lambda}{r_L} U_{out} \quad (2)$$

Where

$$\Lambda = \frac{z_1 z_2 + z_2 z_3 + z_1 z_3}{z_3} \quad (3)$$

In equation (2), when Λ = 0, the output voltage UOUT remains unaffected by RL, resulting in output characteristics akin to a voltage source. Connecting circuit points A, B, and C in Fig. 2(a) to circuit points a, b, and c in Fig. 2(b), respectively, yields the following

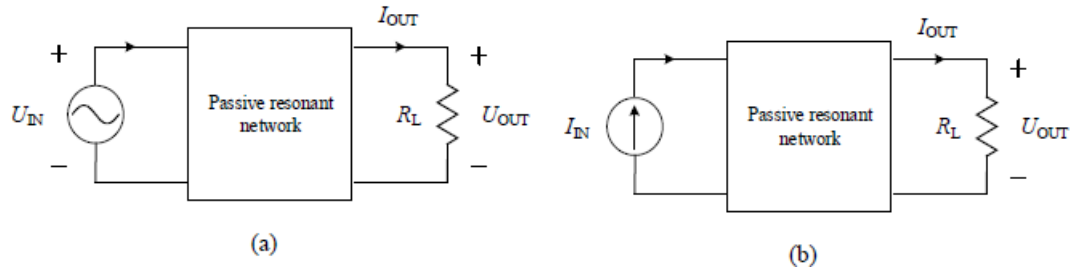


Figure 1 illustrates a resonant circuit featuring (a) a voltage source input and (b) a current source input.

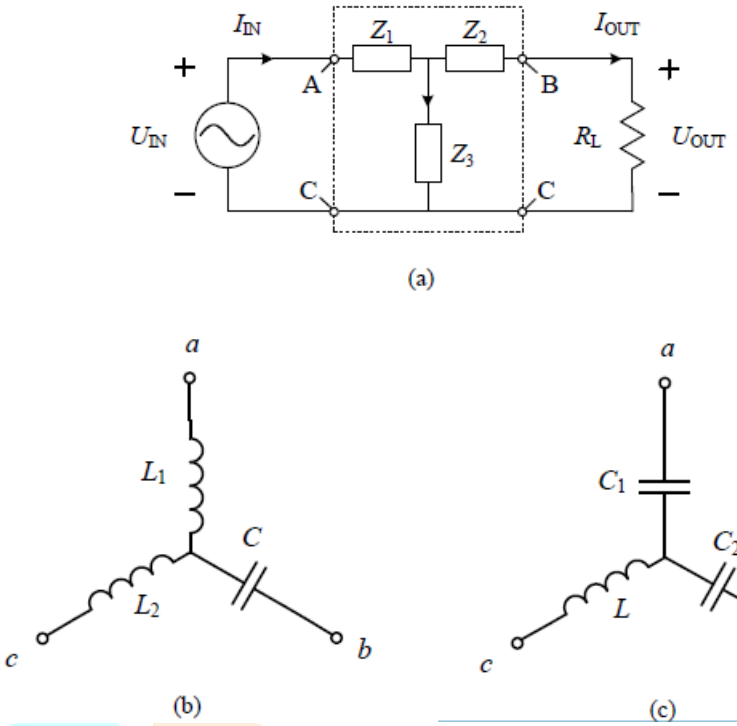


Fig. 2. Resonant network configuration with (a) T circuit model, (b) type A and (c) type B to have constant-voltage output from a voltage source.

$$\Lambda = \frac{l_1 + l_2 - \omega^2 l_1 l_2 C}{j\omega l_2 C} \qquad (4)$$

And $\Lambda = 0$ necessitates the operating frequency of the resonant network to be

$$\omega = \sqrt{\frac{1}{l_1 C} + \frac{1}{l_2 C}} \qquad (5)$$

It maintains a constant-voltage output

$$\frac{U_{out}}{U_{in}} = \frac{l_2}{l_1 + l_2} \qquad (6)$$

If the circuit in Fig. 2(b) is rotated 120 degrees, and circuit points A, B, and C in Fig. 2(a) are connected with circuit points c, b, and a respectively, the circuit can also achieve constant-voltage output at the operating frequency given by (5).

$$\frac{U_{out}}{U_{in}} = \frac{l_1}{l_1 + l_2} \qquad (7)$$

We designate the T-circuit topology in Fig. 2(b), which comprises two resonant inductors and one capacitor, as type A. Similarly, type B configuration with two resonant capacitors and one inductor in Fig. 2(c) can also be employed for constant-voltage output. The operating frequency is provided without derivation,

$$\omega = \frac{1}{\sqrt{lC_1 + lC_2}} \qquad (8)$$

Several typical compensation topologies for constant-voltage output from a voltage source can be summarized based on Fig. 2. The configurations with numbers are listed in Table I.

TABLE I. SUMMARY OF CONSTANT-VOLTAGE OUTPUT FROM A VOLTAGE SOURCE

| Number | Passive resonant network | Resonant frequency |
|---|---|---|
| V-V-1 | 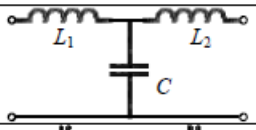 | $\omega = \sqrt{\frac{1}{L_1 C} + \frac{1}{L_2 C}}$ |
| V-V-2 | 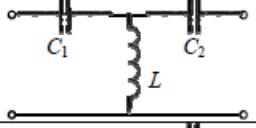 | $\omega = \frac{1}{\sqrt{LC_1 + LC_2}}$ |
| V-V-3 | 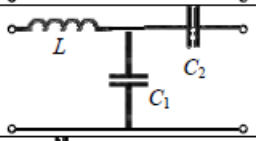 | $\omega = \frac{1}{\sqrt{LC_1 + LC_2}}$ |
| V-V-4 | 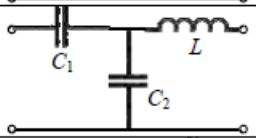 | $\omega = \frac{1}{\sqrt{LC_1 + LC_2}}$ |
| V-V-5 | 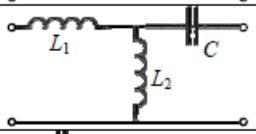 | $\omega = \sqrt{\frac{1}{L_1 C} + \frac{1}{L_2 C}}$ |
| V-V-6 | 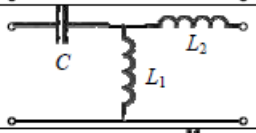 | $\omega = \sqrt{\frac{1}{L_1 C} + \frac{1}{L_2 C}}$ |
| V-V-7 | 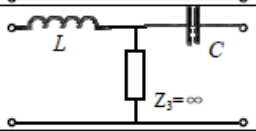 | $\omega = \frac{1}{\sqrt{LC}}$ |
| V-V-8 | 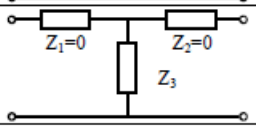 | —— |

Topologies V-V-7 and V-V-8 function as two special cases. In V-V-7, if Z3 = ∞, operating as an open circuit, the output voltage equals the input voltage when L and C resonate at the operating frequency. Meanwhile, for V-V-8, if Z1=Z2=0, constituting a short circuit, the output voltage equals the input voltage irrespective of the value of Z3.

2)Input Current Source:-

If the input is a current source, as shown in Fig. 1 (b), the resonant networks required to achieve a constant-voltage output should have the topologies illustrated in Fig. 3.

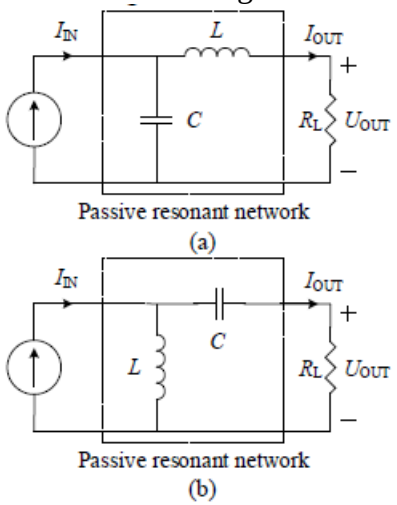


Fig. 3. Resonant circuits (a) type A and (b) type B to have constant-voltage output from a current source.

The output voltage UOUT and input current IIN of type A topology in Fig. 3 (a) can be represented by the 1

$$U_{out} = \frac{1}{j\omega C} i_{IN} - (j\omega l + \frac{1}{j\omega C}) i_{OUT} \qquad (9)$$

It is evident that the second term on the right side of (9) can be eliminated if L and C resonate at the operating frequency, thereby

$$U_{out} = \frac{1}{j\omega C} i_{IN} = -j\omega l i_{IN} \qquad (10)$$

The output voltage is independent of the load, signifying that it is solely determined by the input current and can be adjusted through the resonant components. Type B topology undergoes a comparable analysis process, yielding similar results.

$$U_{out} = j\omega l i_{IN} = -\frac{1}{j\omega C} i_{IN} \qquad (11)$$

The configuration for achieving constant-voltage from a current source are given in Table II

B. Principle of Constant-Current Output

In certain charging applications, the conversion from voltage to current and achieving load-independent current output are desirable. For example, a constant-current output is preferred for driving an LED to maintain stable luminance [52]. The discussion on constant-current output with different input sources is presented below.

TABLE II. SUMMARY OF CONSTANT-VOLTAGE OUTPUT FROM A CURRENT SOURCE

| Number | Passive resonant network | Resonant frequency |
|---|---|---|
| C-V-1 | 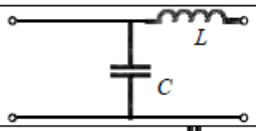 | $\omega = \sqrt{\frac{1}{LC}}$ |
| C-V-2 | 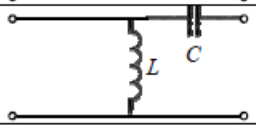 | $\omega = \sqrt{\frac{1}{LC}}$ |

TABLE III. SUMMARY OF CONSTANT-CURRENT OUTPUT FROM A VOLTAGE SOURCE

| Number | Passive resonant network | Resonant frequency |
|---|---|---|
| V-C-1 | 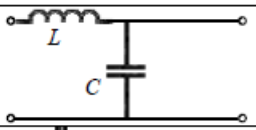 | $\omega = \sqrt{\frac{1}{LC}}$ |
| V-C-2 | 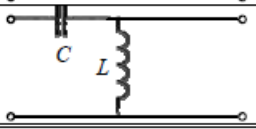 | $\omega = \sqrt{\frac{1}{LC}}$ |

1.Input Voltage Source:-

When the input is a voltage source and a constant-current output is required, it involves the reverse conversion of the topologies listed in Fig. 3. Therefore, the resonant topology employed to achieve the conversion from a voltage source to a constant-current output should also have two types, as listed in Table III. The output currents are

$$V-C-1: i_{out} = \frac{1}{j\omega l} U_{in} = -j\omega C U_{in}$$
$$V-C-2: i_{out} = j\omega C U_{in} = -\frac{1}{j\omega l} U_{in} \qquad (12)$$

2.Input Current Source:-

When the input is a current source, the resonant method for achieving a constant-current output involves a π-circuit configuration, as illustrated in Fig. 4. Similar to achieving a constant-voltage output, to attain a constant-current output from a current source, various compensation topologies can be derived by altering the connections of circuit points A, B, and C in Fig. 4(a) with circuit points a, b, and c in Fig. 4(b) or Fig. 4(c). The derivation is omitted for simplicity, and the configurations are listed in Table IV.

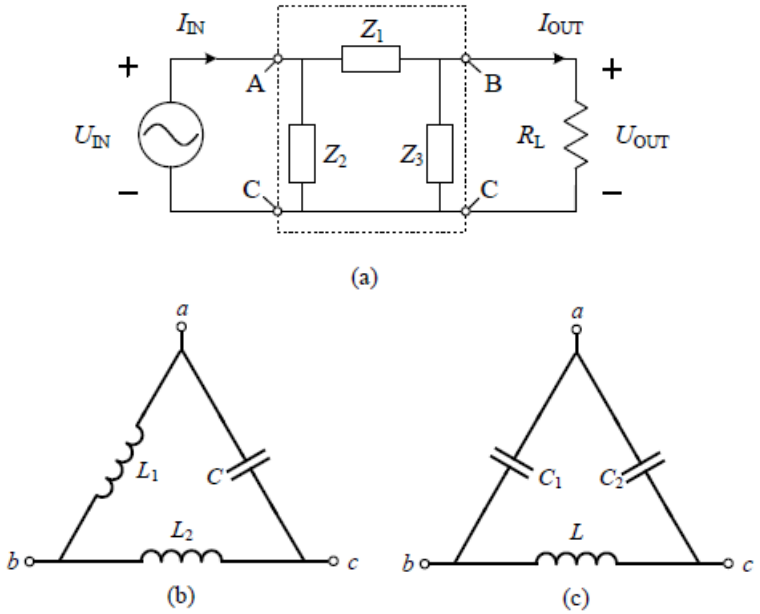


Fig. 4. Resonant network configuration with (a) π circuit model, (b) type A and (c) type B to have constant-current output from a current source.

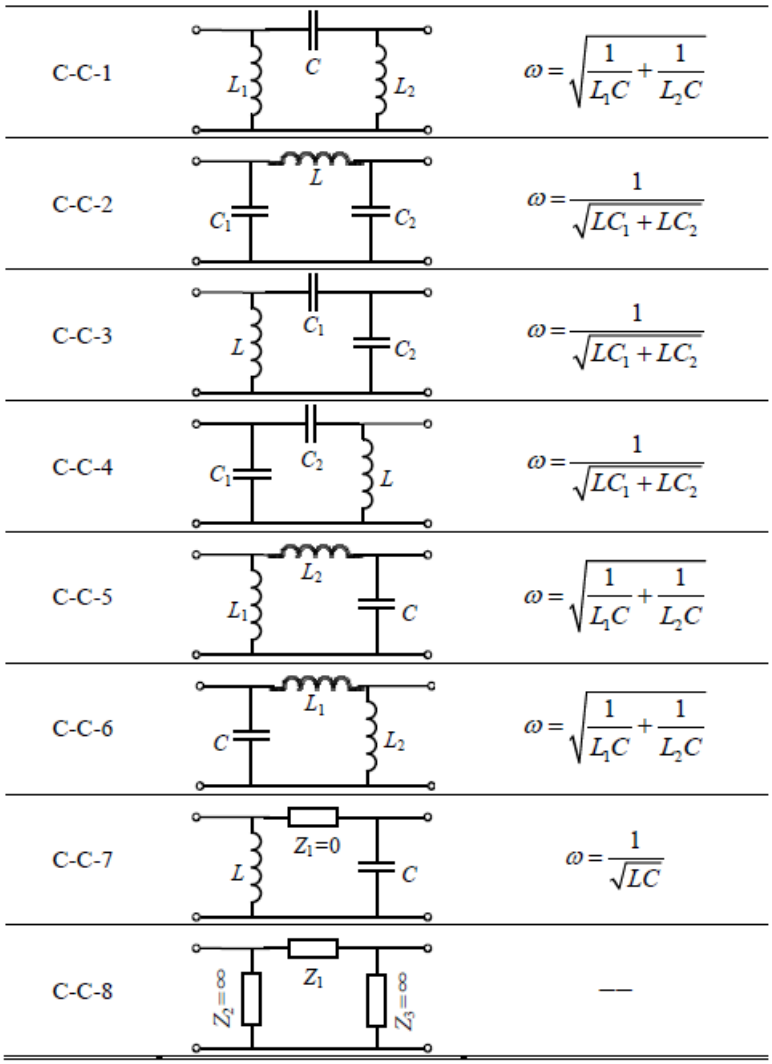


Applications and Examples:-

In this section, various typical compensation topologies capable of achieving constant-voltage output, constant-current output, or both, are examined using the passive resonant networks discussed in Section III. A Wireless Power Transfer (WPT) system operates on the fundamental principle of magnetic induction, similar to other widely used electromechanical devices with good coupling, such as transformers and induction motors. Therefore, the circuit model of a loosely coupled transformer is identical to that of a traditional transformer, as depicted in Fig. 5. For simplicity, the turns-ratio n is selected as 1 in the analysis. LLP and LLS represent the leakage inductances of the primary and secondary. LM is the magnetizing inductance. RPeq

and RSeq denote the resistances of the primary and secondary of the transformer, encompassing the winding resistance and the equivalent resistance of the power loss in the magnetic material. As the values of RPeq and RSeq are relatively small compared to the compensation components' impedances and exert limited influence on the resonant characteristic, they are neglected in this section.

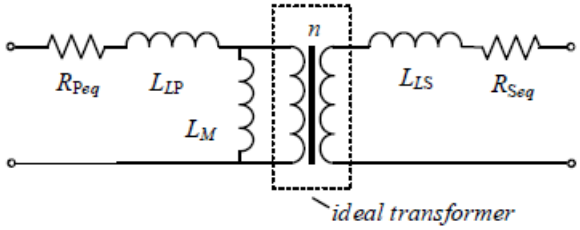


Fig. 5. Loosely coupled transformer circuit model.

A. Series-Series Compensation:-

1)Constant Current Output:-

Primary series and secondary series (S/S) compensation, illustrated in Fig. 6, constitutes one of the four fundamental compensation topologies [28, 40]. CP and CS denote external compensation capacitors in the primary and secondary

Let

$$Z_{lp}(\omega) = j\omega l_{lp} + \frac{1}{j\omega C_p}$$
$$Z_{ls}(\omega) = j\omega l_{ls} + \frac{1}{j\omega C_s} \qquad (13)$$

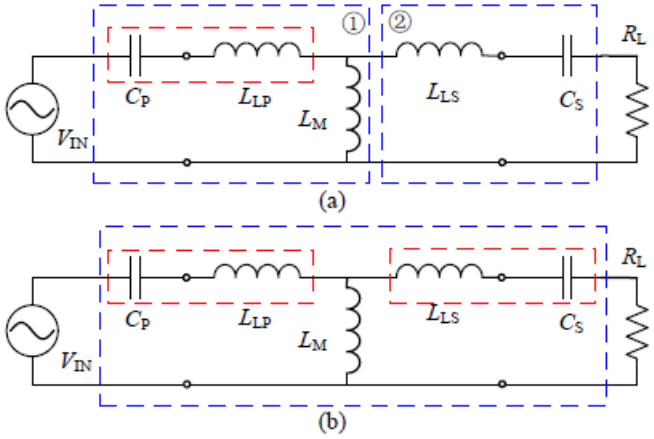


Fig. 6. Primary series and secondary series compensation circuit models to realize (a) constant-current and (b) constant-voltage output

Usually, the S/S compensation is designed to maintain a constant-current output [28], and the operating frequency is unique. This can be elucidated by the resonant networks in Section III. Referring to Fig. 6 (a), if ZLP(ω) < 0 and the resonant tank in the red block is equivalent to a capacitor, which can resonate with LM, then block ① can be treated as the resonant network V-C-2 in Table III. Consequently, a constant-current is achieved in the branch circuit parallel with LM. Therefore, the output current remains constant irrespective of the values of LLS, CS, and RL, as block ② can be viewed as the resonant circuit C-C-8 in Table IV, which yields a constant-current output from the current source generated by block ①. The unique resonant frequency for achieving constant-current output is

$$\omega = \omega_p = \frac{1}{\sqrt{(l_{lp} + l_m)C_p}} = \frac{1}{\sqrt{l_p C_p}} \qquad (14)$$

Where $L_p$ is the self inductance of the primary coil

2.Constant Voltage Output:-

The S/S topology can also be compensated to achieve constant-voltage output, and the operating frequency for realizing constant-voltage output is not unique. If we choose the compensation capacitors CP and CS randomly, two situations may exist:

a) An operating frequency ωH can be found to have ZLP(ω) = ZLS(ω) = 0. Operating at ωH, the S/S topology can be regarded as the resonant circuit V-V-8 in Table I. If ωH exists, a frequency area should also exist, in which ZLP(ω) < 0 and ZLP(ω) < 0. The series-connected resonant components in both the primary and secondary are both equivalent with capacitors. A frequency ωL can be found to create the resonant circuit V-V-2 in Table I. Therefore, ωH and ωL are the two frequencies that realize constant-voltage output.

b) An operating frequency cannot be found to have ZLP(ω) = ZLS(ω) = 0. In this situation, the operating frequency can be adjusted within a certain range such that ZLP(ω) > 0 and ZLS(ω) < 0, or within a range such that ZLP(ω) < 0 and ZLS(ω) > 0. Only one of these two scenarios can be achieved with one group of circuit parameters. Therefore, one operating frequency exists such that at ωH the resonant circuit operates as V-V-5 (when ZLP(ω) > 0 and ZLS(ω) < 0) or V-V-6 (when ZLP(ω) < 0 and ZLS(ω) > 0) in Table I. Simultaneously, with the same group of circuit parameters, another operating frequency can always be found to have ZLP(ω) < 0 and ZLS(ω) < 0. Therefore, the other operating frequency exists such that at ωL the resonant circuit operates as V-V-2 in Table I.]

These two frequencies can also be determined through mathematical equations. To ensure the applicability of the derivation for a general loosely coupled transformer, as opposed to those with n=1, the turn ratio is introduced in the analysis below. However, in the subsequent figures, a transformer with n=1 is retained to facilitate a clear explanation involving the blocks of resonant circuits in Section III.

The output voltage on $R_L$ is calculated as

$$U_{out} = U_{in} G_V \qquad (15)$$

Where $G_V$ is the voltage transfer ratio, which can then be represented as

$$G_V = \frac{U_{out}}{U_{in}} = \frac{j\omega n l_m r_L}{z_P z_S + n^2 \omega^2 l_m^2} \qquad (16)$$

Where $Z_S$ is the impedance of secondary resonant tank that includes load resistance $R_L$. $Z_p$ is the impedance of primary resonant tank where $L_p$ and $L_S$ are the self-inductances

$$z_S = j\omega l_S + \frac{1}{j\omega C_S} + r_L$$
$$z_P = j\omega l_P + \frac{1}{j\omega C_P} \qquad (17)$$

The voltage transfer characteristics can be obtained by further modification of (16)

$$G_V = \frac{1}{\frac{z_P}{\omega n l_m} + \frac{\delta}{\omega^3 n l_m C_P C_S r_L}} \qquad (18)$$

$$\delta = \omega^4 l_p C_p l_s C_s (k^2 - 1) + \omega^2 (l_p C_p + l_s C_s) - 1 \qquad (19)$$

Where $k = \frac{n l_m}{\sqrt{l_P l_S}}$ is coupling coefficient of loosely coupled transformer. From equation (19) we can see if $\delta$ =0, then mod of $G_v$ is load-independent and output voltage remains constant when values of $R_L$ changes.

Solving for roots of $\delta$ =0, the frequencies at which mod of $G_V$ is independent of $R_L$ can be obtained from

$$\omega_l = \sqrt{\frac{\omega_p^2 + \omega_s^2 - \Delta}{2(1-k^2)}} \qquad (20)$$

$$\omega_h = \sqrt{\frac{\omega_p^2 + \omega_s^2 + \Delta}{2(1-k^2)}} \qquad (21)$$

$$\Delta = \sqrt{(\omega_p^2 + \omega_s^2)^2 - 4(1-k^2)\omega_p^2 \omega_s^2} \qquad (22)$$

Where $\omega_s = \frac{1}{\sqrt{l_s C_s}}$ is resonant frequency of $l_S$ and $C_s$.$l_S$ is self-inductance of secondary coil.So existence of $\omega_L$ and $\omega_H$ is verified.

In the study conducted by [45], a comparison is made between self-inductance compensation and leakage inductance compensation. The sole distinction between these two compensations lies in the values of the capacitors. Hence, based on the preceding analysis, it can be concluded that both types of compensation can attain constant-voltage/current output, albeit operating at different frequencies.

B. Parallel-Series Compensation: -

Primary series and secondary parallel (S/P) compensation is typically configured to maintain a constant-voltage output. Referring to Fig. 7 (a), if ZLP(ω) < 0, the S/P compensation topology can be treated as the amalgamation of the resonant network V-V-6 in block ① and V-V-8 in block ②. The realization of a constant-voltage output is possible only when operating at

$$\omega = \sqrt{\frac{1}{C_P(l_{lp} + \frac{l_m l_{ls}}{l_m + l_{ls}})}} \qquad (23)$$

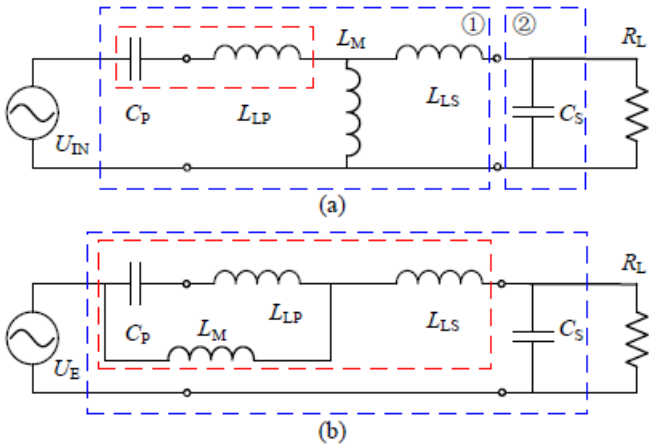


Fig. 7. Primary series and secondary parallel (S/P) compensation circuit models to have (a) constant-voltage and (b) constant-current output (Thévenin's equivalent circuit).

S/P compensation can also achieve constant-current output. Through additional manipulation using Thévenin's equivalent circuit, the S/P compensation topology can be rearranged as depicted in Fig. 7 (b), demonstrating constant-current output. Here, UE represents the equivalent input voltage after Thévenin's conversion.

$$U_e = U_{in} \frac{j\omega l_m}{z_p} \qquad (24)$$

If the operating frequency is chosen such that the impedance in the red dotted block functions as an equivalent inductor, capable of resonating with CS, it can be considered as the resonant circuit V-C-1 in Table III, resulting in a constant output current. The transconductance ratio can be derived.

$$G_i = \frac{I_{out}}{I_{in}} = \frac{1}{\omega n l_m + \frac{j\omega l_s z_p}{\omega n l_m} + \gamma r_L} \qquad (25)$$

Where,

$$\gamma = j\omega^2 n l_m C_S + \frac{z_P(1-\omega^2 l_s C_S)}{\omega n l_m} \qquad (26)$$

Similarly, ensuring that γ=0 at specific frequencies guarantees that IO is independent of RL. It has been observed that ωL and ωH in equations (20) and (21) also serve as the two roots of γ=0 [47]. Consequently, ωL and ωH represent the frequencies at which S/P compensation accomplishes load-independent current output.

Primary LCC Compensations: -

The design of primary LCC series–parallel compensations is intended for Wireless Power Transfer (WPT) systems with multiple loadings, such as roadway-powered vehicle Inductive Power Transfer (IPT) systems. These systems are composed of a primary track, consisting of an elongated loop that serves as the primary component of the loosely coupled transformer. The primary track is tasked with supplying power wirelessly to several independent loads, typically electric vehicles, each of which couples to the track via a pickup inductor placed in proximity to the track wires. Therefore, maintaining constant track current is essential to ensure consistent power delivery to each pickup system [5, 29].

A series of primary LCC series–parallel compensations, as illustrated in Fig. 8, finds widespread application in the design of track WPT systems [29, 49]. The variable Itrack represents the current flowing through the track, and the design objective is to sustain a constant Itrack during operation. Simultaneously, each load powered by the track should have either constant voltage or constant-current output.

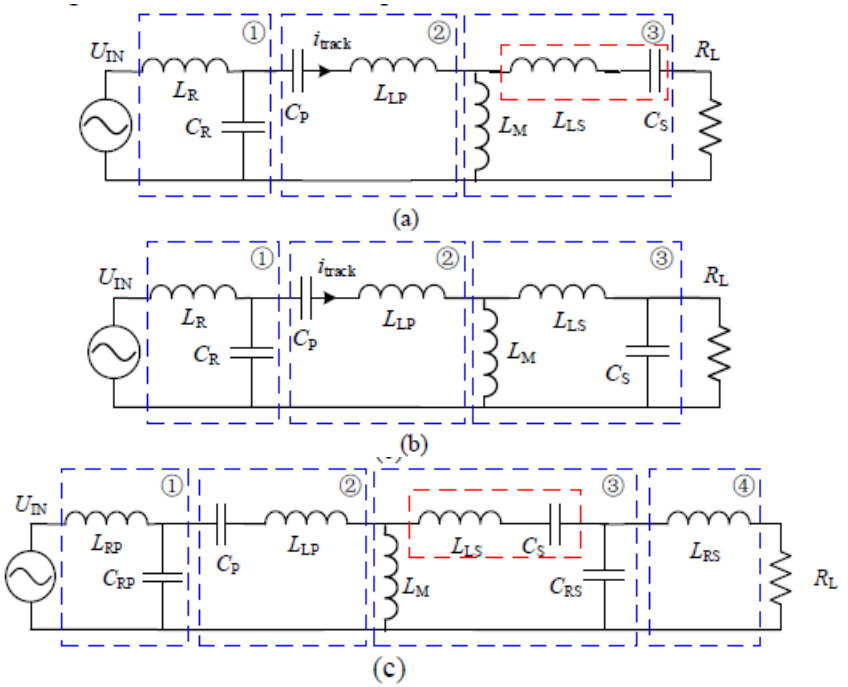


Fig. 8. Primary LCC series–parallel-compensation circuit models with (a) secondary series compensation, (b) secondary parallel compensation and (c) secondary LCC compensation

In the case of all primary LCC series–parallel compensations, achieving constant current in the primary coil is feasible when LR and CR in block ① are appropriately chosen to resonate at the operating frequency of the converter. The primary LCC series–parallel compensation topology, illustrated in block ① of Fig. 8, can be considered analogous to the resonant circuit V-C-1 in Table III. Treating the constant current of the primary coil as a current source, block ② represents the resonant circuit CC-8.

For achieving constant voltage on the load in the secondary of the transformer, a compensation capacitor should be connected in series with the secondary coil, as depicted in Fig. 8 (a). In this configuration, block ③ corresponds to C-V-1, and CS resonates with LM+LLS. Therefore, achieving constant-voltage output necessitates:

$$\omega = \frac{1}{\sqrt{(l_{ls}+l_m)C_s}} = \frac{1}{\sqrt{l_s C_s}} = \frac{1}{\sqrt{l_R C_R}} \qquad (27)$$

If the compensation capacitor is connected in parallel with the secondary coil, as depicted in Fig. 8 (b), a resonant network C-C-1 is formed in block ③, allowing for the attainment of constant current when satisfying condition (27). In [53], a double-sided LCC compensation topology is introduced, illustrated in Fig. 8(c), featuring symmetrical compensation in both the primary and secondary. By incorporating a capacitor in block ③ (C-C-1) and a block ④ (C-C-8), constant current output is achieved.
In applications such as battery chargers, an additional converter is commonly positioned on the secondary side to manage the battery load profile, involving a first step at constant-current and a second one at constant-voltage [54]. Through the use of appropriate compensations and controlled operating frequency selection, a single stage of Wireless Power Transfer (WPT) converter can facilitate voltage or current conversion.

## V. Achieving Zero Phase Angle and Soft Switching

The phase angle θin, determining the relationship between the input voltage and current, plays a crucial role in deciding the Volt-Ampere (VA) rating of the power supply and the switching components. Additionally, it is integral to achieving soft switching in an H-bridge converter. The minimum VA rating necessitates θin to be equal to zero, while ensuring soft switching for MOSFETs requires θin to be greater than zero. Hence, θin is typically chosen to be slightly greater than zero to facilitate the achievement of soft-switching, along with maintaining a reasonable Volt-Ampere (VA) rating.

The input phase angle is calculated as

$$\theta_{in} = \frac{180}{\pi} \tan^{-1} \frac{\mathrm{Im}(z_{in})}{\mathrm{Re}(z_{in})} \qquad (28)$$

We have studied the condition of $\theta_{in}$ =0. It can be achieved when Im($Z_{in}$)= 0.

As per the analysis of passive resonant networks in Section III, due to the variation in the loading resistance, which is connected in parallel with one of the resonant components, maintaining θin = 0 with only one stage of passive resonant network is not feasible. However, two special topologies, V-V-7 and C-C-7, serve as exceptions. Let's consider the S/S compensation topology as an illustration. Referring to Fig. 6 (b), if the S/S compensation is configured for constant-voltage output, given it has only one stage of resonant block, the value of θin becomes dependent on the loading resistances. θin can exhibit positive or negative values with varying RL [55]. Consequently, the S/S compensation topology cannot achieve ZPA when configured for constant-voltage output

To achieve both load-independent voltage/current output and θin = 0 across the entire loading range, the utilization of two or more stages of resonant circuits, as explored in Section III, becomes necessary. Illustrated in Fig. 6 (a), when S/S compensation is configured for constant-current output, it involves the combination of two resonant networks, namely V-C-2 and C-C-8. Although Stage C-C-8 does not directly contribute to the creation of a constant-current, it possesses the capability to adjust the value of θin. Consequently, S/S compensation can concurrently achieve input ZPA and constant-current output [47].

A primary series and secondary series-parallel compensated topology (S/SP) is proposed as an enhancement to the S/S compensation topology, aiming to achieve ZPA and constant-voltage output simultaneously [56]. In the S/SP circuit illustrated in Fig. 9, CP and CS are deliberately chosen to be identical, forming the resonant network depicted in Fig. 6 (b). To realize an additional stage of V-V-8, a secondary parallel-connected capacitor CSP is introduced. Although this stage doesn't contribute to constant-voltage output, CSP plays a crucial role in controlling and adjusting θin for the S/SP compensation, thereby facilitating the realization of soft-switching.

$$C_{sp} = \frac{1}{\omega^2 n^2 l_m} \tag{29}$$

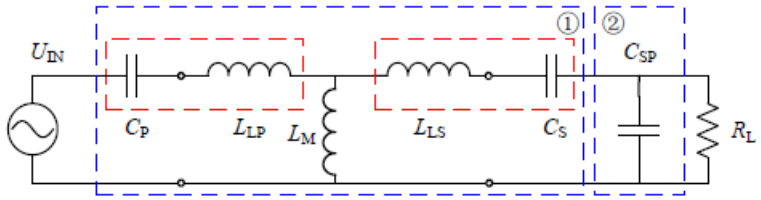


Fig. 9. Primary series and secondary series-parallel (S/SP) compensation circuit model.

Similarly, S/P compensation also encounters this issue. In the resonant circuit V-C-1 depicted in Fig. 7 (b), which constitutes the single stage adapted for constant-current output, an additional stage of the resonant network is required to achieve ZPA for all loads and ensure load-independent current output simultaneously. Fig. 10 illustrates the resonant network with V-C-1 and the supplementary stage. This additional stage can be introduced either before or after the V-C-1 stage, and we consider both scenarios for a comprehensive analysis of all possible circuit topologies. In practical applications, selecting either jXa=∞ or jXb=0 can represent one stage.

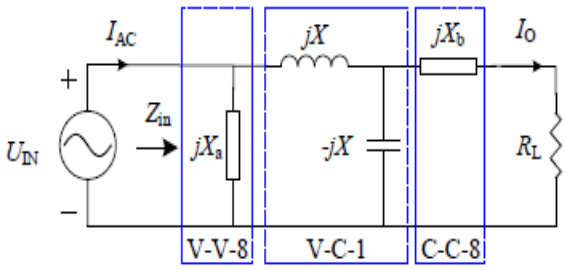


Fig. 10. Two or more stages (including V-C-1) to have constant-current output as well as input ZPA.

Since the capacitor and inductor in the stage of V-C-1 resonate with each other so let

$$X = \omega l = \frac{1}{\omega C} \tag{30}$$

And,

$$z_{in} = \frac{r_L X^2 X_a^2 + jX^2 X_a[X^2 + X_a(X - X_b)]}{[X^2 + X_a(X - X_b)]^2 + r_L^2 X_a^2} \quad (31)$$

If $X_a \to \infty$,then C-C-8 has been added behind the V-C-1 stage,

$$z_{in} = \frac{r_L X^2 + jX^2(X - X_b)}{r_L^2} \quad (32)$$

To realize Im($Z_{in}$)=0 and $\theta_{in}$ =0, $X_b$ should be equal to X. If $X_b$=0, then V-V-8 has added before V-C-1 stage, and

$$z_{in} = \frac{r_L X^2 X_a^2 + jX^2 X_a[X^2 + X_a X]}{[X^2 + X_a X]^2 + r_L^2 X_a^2} \quad (33)$$

To achieve $\theta_{in}$ equal to 0, Xa must be equal to -X. If the stages of both V-V-8 and C-C-8 are combined, then, in accordance with (31), the impedances should meet the following condition:

$$X^2 + X_a(X - X_b) = 0 \quad (34)$$

In order to make $\theta_{in}$= 0 for all loading conditions

In all primary LCC series–parallel compensations, given their utilization of V-C-1 or V-C-2 resonant networks to achieve constant current in the primary coil, the series-connected capacitor CP (as seen in Fig. 8) can be considered as an additional stage C-C-8. Although this stage does not contribute to constant current, it is included to adjust θin. In accordance with (31), the attainment of ZPA is possible when:

$$C_p = \frac{C_R}{\frac{l_P}{l_R} - 1} \quad (35)$$

SYSTEM EFFICIENCY:-

To calculate system efficiency, the resistances $R_{Peq}$ and $R_{Seq}$ in Fig 5 should considered. Then $Z_P$ and $Z_S$ redefined as:-

$$z_S = j\omega l_S + \frac{1}{j\omega C_S} + r_{Seq} + r_L$$

$$z_P = j\omega l_P + \frac{1}{j\omega C_P} + r_{Peq}$$

The calculation of power transfer efficiency can be derived by exclusively considering the active power, as demonstrated in [47, 54]. Consequently, the efficiency ηP of the primary loop and the efficiency ηS of the secondary loop can be computed independently as:

$$\eta_P = \frac{\mathrm{Re}(z_{ref})}{r_{Peq} + \mathrm{Re}(z_{ref})} \quad (36)$$

$$\eta_S = \frac{\mathrm{Re}(z_s) - r_{seq}}{\mathrm{Re}(z_S)} \quad (37)$$

$z_{ref}$ is reflected impedance from secondary to primary

$$z_{ref} = \frac{\omega^2 n^2 l_m^2}{z_S} \quad (38)$$

The efficiency $\eta$ is given by

$$\eta = \eta_P . \eta_S \quad (39)$$

From (36) to (39), the circuit efficiency is tied to $R_{Peq}$, $R_{Seq}$, $nL_M$, and $Z_S$. If the operating frequency remains fixed or varies within a narrow range, $RP_{eq}$ and $R_{Seq}$ are associated with the chosen electric wire and magnetic material. The term $nL_M$ represents mutual inductance and is determined by the coupling coefficient of the transformer. These parameters can be considered constant once the loosely coupled transformer is constructed, and they are not discussed in this paper.

Hence, ZS becomes the sole determinant of circuit efficiency. If the compensation capacitors possess no equivalent series resistance (ESR), the efficiency, as derived from (36) to (39), is independent of the primary compensation network. Primary compensation solely influences the reactive power of the circuit, the Volt-Ampere (VA) rating of the input power source, and the realization of soft-switching. As per (38), ZS is influenced by 1) the impedance of the secondary resonant network and 2) the value of the loading resistance. For a given transformer, adjusting these two parameters, which determine ZS, allows for the achievement of maximum circuit efficiency.

Regarding the impedance of the secondary resonant network, the compensation capacitor should be meticulously designed to realize maximum efficiency. According to the findings in [47, 54], the pinnacle of efficiency is reached when:

$$\text{Secondary series compensation } C_s = \frac{1}{\omega^2 l_S}$$

$$\text{Secondary parallel compensation } C_s = \frac{1}{\omega^2 l_S \Gamma^2} \qquad (40)$$

Where ,

$$\Gamma = (1+\frac{Q_p}{Q_s}k^2)^{\frac{1}{4}} \qquad (41)$$

$Q_P$ and $Q_S$ are defined as winding quality factor which can be expressed as

$$Q_p = \frac{\omega l_P}{r_{Peq}} \text{ and } Q_s = \frac{\omega l_s}{r_{Seq}} \qquad (42)$$

Therefore, to attain maximum efficiency, the capacitor in the secondary resonant network should be configured as specified in equation (40). Regarding the loading resistance, if RL is represented in terms of the circuit quality factor QL, based on the findings in [47, 54], the requirement for achieving maximum efficiency is that QL should satisfy the following condition:

$$Q_L = \frac{Q_s}{\sqrt{1+k^2 Q_p Q_s}} \qquad (43)$$

for both secondary series and parallel compensations. The expression for the circuit quality factor QL in equation (43) varies between secondary series and parallel compensations.

$$\text{Secondary series compensation } Q_L = \frac{1}{r_L}\sqrt{\frac{l_s}{C_s}}$$

(44)

$$\text{Secondary parallel compensation } Q_L = r_L\sqrt{\frac{C_s}{l_s}}$$

Considering the imperative to attain maximum efficiency, secondary series and parallel compensations find application in diverse scenarios. Take, for example, the context of Electric Vehicle (EV) battery wireless charging. Assuming the onboard battery has a voltage of 400V and an internal resistance of 0.7 ohms, and the recharging power is 3.3kW for private cars, a straightforward derivation yields an output voltage and current requirement of 405.7V and 8.13A, respectively. Consequently, the equivalent loading resistance RL is determined to be 49.9 ohms. Utilizing proper litz wire, the winding quality factors QP and QS can typically achieve a value of 200, while the assumed coupling coefficient is 0.2.

Applying equation (43), the quality factor QL is calculated to be 5. Subsequently, employing equation (44), if secondary series compensation is chosen, the inductance value LS is determined to be 468 μH when the converter operates at 85 kHz. On the other hand, selecting secondary parallel compensation necessitates designing LS as 18 μH. However, given the practical constraints of installing a coil on the chassis of a vehicle and with a coupling coefficient k=0.2, 18 μH is deemed an impractical value. Therefore, for this EV wireless charging example, secondary series compensation is deemed more suitable to achieve maximum efficiency.]

In general, when taking into account the Equivalent Series Resistances (ESRs) of compensation conductors and capacitors, an increase in the number of compensation components tends to result in lower circuit efficiency. S/S and S/P compensation circuits exhibit the highest efficiencies, attributed to the utilization of only two compensation components. Systems employing S/S and S/P compensations demonstrate nearly identical maximum efficiencies [47], and ηmax can be expressed as follows:

$$\eta_{\max} = \frac{c}{(1+\sqrt{1+c})^2} \qquad (45)$$

$$c = k^2 Q_P Q_S$$

The attainment of maximum efficiency, denoted as ηmax, is contingent upon satisfying both equations (40) and (43), and is solely dependent on the values of k and the winding quality factors. A loosely coupled transformer, as depicted in Fig. 11, was constructed to validate the circuit efficiency of a 3.3kW stationary Electric Vehicle (EV) wireless charging prototype. The transformer specifications are detailed in Table V. To calculate the system efficiency, a quality factor of QP=QS=200 is selected, representing a typical value for a loosely coupled transformer operating at around 85 kHz. The double-sided LCC compensation topology illustrated in Fig. 8(c) is employed for experimentation. For the compensation inductor in the circuits, using the same wire as the loosely coupled transformer, the quality factor of the resonant inductor is also set at 200, and the capacitor has a dissipation factor (DF) of 0.05%, as per the datasheet. The circuit efficiency is both measured and calculated. The calculated system efficiency (DC-DC) is 93.6%, while the measured efficiency is 92.6%. The consistency between measurement and calculation confirms the accuracy of the QP, QS, and ESR values of the compensation components.

TABLE V. SPECIFICATIONS OF THE LOOSELY COUPLED TRANSFORMER PROTOTYPE

| Transformer & circuit parameters | | Specifications |
|---|---|---|
| Coil topology | | Unipolar |
| coil | primary | Circular, 600 mm dia., 32 turns, litz wire with 800 strands AWG38, two wires connected in parallel as one turn, $L_P$= 420 μH |
| | secondary | Circular, 300 mm dia., 16 turns, litz wire with 800 strands AWG38, $L_S$= 110 μH |
| core | primary | 48 bars of PC40 with 8mm thickness, same external diameter with the primary coil. |
| | secondary | 48 bars of PC40 with 8mm thickness, same external diameter with the secondary coil. |
| Shieldings | | 2 mm aluminum circular sheet, same size with the coil |
| Air gap | | 150 mm |
| Coupling coefficient | | 0.182 |
| Output power | | 3.3 kW |
| Battery voltage | | 400 V |
| Input voltage | | 350 V |
| Operating frequency | | 85 kHz |

Under identical conditions of a loosely coupled transformer and equivalent values for compensation components ESR, the efficiencies of different compensation topologies are computed and presented in Table VI. The results affirm that S/S and S/P compensations exhibit superior efficiencies compared to other topologies, validating the precision of equation (45).

TABLE VI. MAXIMUM EFFICIENCIES OF DIFFERENT COMPENSATION TOPOLOGIES

| Compensation topology | Maximum efficiency | Constant output type |
|---|---|---|
| Series-series | 94.6% | current |
| Series-parallel | 94.6% | voltage |
| Series-series with leakage inductance compensation | 93.3% | voltage |
| LCC-series | 94.2% | voltage |
| LCC-parallel | 94.3% | current |
| LCC-LCC | 93.5% | current |

The efficiency of the S/S topology with leakage-inductance compensation is computed under the stipulation of maintaining a constant-voltage output, as originally intended [45]. The operational frequency, corresponding to constant-voltage output, is denoted as either ωL or ωH in equations (19) and (20), distinct from the secondary resonant frequency specified in equation (40) for achieving maximum efficiency. Consequently, the S/S topology with leakage-inductance compensation, aiming for constant-voltage output, exhibits lower efficiency compared to self-inductance compensation targeting constant-current output.]

Conclusion: - The introduction of the constant-current/voltage output function in a passive resonant network is based on individual resonant blocks. These fundamental resonant blocks serve to elucidate various characteristics of contemporary compensation topologies, encompassing constant-voltage or constant-current output, the realization of input zero phase angle, and the implementation of soft-switching. Through the judicious combination of these resonant blocks, it becomes possible to create any type of compensation topology, ensuring a simultaneous Wireless Power Transfer (WPT) rating. Additionally, the analysis of system efficiency involves studying different resonant circuits, and a review of the compensation conditions required to achieve maximum efficiency is conducted. A rational circuit design, taking into consideration the WPT system's application area, is essential for attaining this optimal efficiency. Furthermore, primary-series and secondary-series topologies with leakage-inductance compensation and self-inductance compensation are studied and compared.

**References**

**[1]** http://en.wikipedia.org/wiki/Wardenclyffe. 2014.
2. Tesla, N., *Apparatus for transmitting electrical energy*. 1914, US Patent 1119732.
3. Tesla, N., *My Inventions: The Autobiography of Nikola Tesla*. 2005: Wildside Press.
4. Lomas, R., *The Man Who Invented the Twentieth Century.: Nikola Tesla, Forgotten Genius of Electricity*. 2000: Headline Book Publishing.
5. Covic, G.A. and J.T. Boys, *Inductive Power Transfer.* Proceedings of the IEEE, 2013. **101**(6): p. 1276-1289.
6. Xun, L. and S.Y.R. Hui, *Equivalent Circuit Modeling of a Multilayer Planar Winding Array Structure for Use in a Universal Contactless Battery Charging Platform.* IEEE Transactions on Power Electronics, , 2007. **22**(1): p. 21-29.
7. Xun, L. and S.Y.R. Hui, *Optimal Design of a Hybrid Winding Structure for Planar Contactless Battery Charging Platform.* IEEE Transactions on Power Electronics, , 2008. **23**(1): p. 455-463.
8. Yungtaek, J. and M.M. Jovanovic, *A contactless electrical energy transmission system for portable-telephone battery chargers.* IEEE Transactions on Industrial Electronics, , 2003. **50**(3): p. 520-527.
9. Dissanayake, T.D., et al., *Experimental Study of a TET System for Implantable Biomedical Devices.* IEEE Transactions on Biomedical Circuits and Systems, , 2009. **3**(6): p. 370-378.
10. Ho Yan, L., D.M. Budgett, and A.P. Hu, *Minimizing Power Loss in Air-Cored Coils for TET Heart Pump Systems.* IEEE Journal on Emerging and Selected Topics in Circuits and Systems,, 2011. **1**(3): p. 412-419.
11. Nishimura, T.-H., et al. *A large air gap flat transformer for a transcutaneous energy transmission system*. in *25th Annual IEEE Power Electronics Specialists Conference, PESC '94*. 1994.
12. Takura, T., et al., *Basic evaluation of signal transmission coil in transcutaneous magnetic telemetry system for artificial hearts.* IEEE Transactions on Magnetics, , 2005. **41**(10): p. 4173-4175.

13. Miura, H., et al., *Improvement of the Transcutaneous Energy Transmission System Utilizing Ferrite Cored Coils for Artificial Hearts.* IEEE Transactions on Magnetics,, 2006. **42**(10): p. 3578-3580.
14. Xun, L. and S.Y.R. Hui, *Simulation Study and Experimental Verification of a Universal Contactless Battery Charging Platform With Localized Charging Features.* IEEE Transactions on Power Electronics, , 2007. **22**(6): p. 2202- 2210.
15. Chang-Gyun, K., et al., *Design of a contactless battery charger for cellular phone.* IEEE Transactions on Industrial Electronics, , 2001. **48**(6): p. 1238- 1247.
16. Waffenschmidt, E. and T. Staring. *Limitation of inductive power transfer for consumer applications*. in *13th European Conference on Power Electronics and Applications, 2009.* . 2009.
17. Hui, S.Y.R. and W.W.C. Ho, *A new generation of universal contactless Battery Charging platform for portable Consumer Electronic equipment.* IEEE Transactions on Power Electronics, , 2005. **20**(3): p. 620-627.
18. Hui, S.Y., *Planar Wireless Charging Technology for Portable Electronic Products and Qi.* Proceedings of the IEEE, 2013. **101**(6): p. 1290-1301.
19. Ghahary, A. and B.H. Cho, *Design of transcutaneous energy transmission system using a series resonant converter.* IEEE Transactions on Power Electronics, , 1992. **7**(2): p. 261-269.
20. Gyu Bum, J. and B.H. Cho, *An energy transmission system for an artificial heart using leakage inductance compensation of transcutaneous transformer.* IEEE Transactions on Power Electronics, , 1998. **13**(6): p. 1013-1022.
21. Kissin, M.L.G., H. Hao, and G.A. Covic. *A practical multiphase IPT system for AGV and roadway applications*. in *IEEE Energy Conversion Congress and Exposition (ECCE), 2010* 2010.
22. Zaheer, A., et al. *Magnetic design of a 300 W under-floor contactless Power Transfer system*. in *37th Annual Conference on IEEE Industrial Electronics Society*. 2011.
23. Basset, P., et al., *Complete System for Wireless Powering and Remote Control of Electrostatic Actuators by Inductive Coupling.* IEEE/ASME Transactions on Mechatronics, , 2007. **12**(1): p. 23-31.
24. Jeroen de, B., E.A. Lomonova, and A.J.A. Vandenput, *Optimization of Contactless Planar Actuator With Manipulator.* IEEE Transactions on Magnetics, , 2008. **44**(6): p. 1118-1121.
25. Zhang, W., et al., *An Optimized Track Length in Roadway Inductive Power Transfer Systems.* IEEE Journal of Emerging and Selected Topics in Power Electronics,, 2014. **PP**(99): p. 1-1.
26. Villa, J.L., et al., *Design of a high frequency Inductively Coupled Power Transfer system for electric vehicle battery charge.* Applied Energy, 2009. **86**(3): p. 355-363.
27. Musavi, F., M. Edington, and W. Eberle. *Wireless power transfer: A survey of EV battery charging technologies*. in *IEEE Energy Conversion Congress and Exposition (ECCE), 2012* 2012.
28. Sungwoo, L., et al. *On-Line Electric Vehicle using inductive power transfer system*. in *IEEE Energy Conversion Congress and Exposition (ECCE), 2010*. 2010.
29. Sungwoo, L., C. Bohwan, and C.T. Rim, *Dynamics Characterization of the Inductive Power Transfer System for Online Electric Vehicles by Laplace Phasor Transform.* IEEE Transactions on Power Electronics,, 2013. **28**(12): p. 5902-5909.
30. Sato, F., et al., *Contactless energy transmission to mobile loads by CLPS-test driving of an EV with starter batteries.* IEEE Transactions on Magnetics, 1997. **33**(5): p. 4203-4205.
31. Garnica, J., R.A. Chinga, and L. Jenshan, *Wireless Power Transmission: From Far Field to Near Field.* Proceedings of the IEEE, 2013. **101**(6): p. 1321-1331.
32. Ghahary, A. and B.H. Cho. *Design of a transcutaneous energy transmission system using a series resonant converter*. in *21st Annual IEEE Power Electronics Specialists Conference, 1990.* . 1990.
33. Erickson, R.W. and D. Maksimovic, *Fundamentals of Power Electronics*. 2001: Springer.
34. Kissin, M.L.G., G.A. Covic, and J.T. Boys, *Steady-State Flat-Pickup Loading Effects in Polyphase Inductive Power Transfer Systems.* IEEE Transactions on Industrial Electronics, , 2011. **58**(6): p. 2274-2282.
35. Kutkut, N.H., et al., *Design considerations and topology selection for a 120- kW IGBT converter for EV fast charging.* IEEE Transactions on Power Electronics, , 1998. **13**(1): p. 169-178.
36. Chwei-Sen, W., G.A. Covic, and O.H. Stielau, *Investigating an LCL load resonant inverter for inductive power transfer applications.* IEEE Transactions on Power Electronics,, 2004. **19**(4): p. 995-1002.
37. Keeling, N.A., G.A. Covic, and J.T. Boys, *A Unity-Power-Factor IPT Pickup for High-Power Applications.* IEEE Transactions on Industrial Electronics, 2010. **57**(2): p. 744-751.
38. Elliott, G.A.J., et al., *A New Concept: Asymmetrical Pick-Ups for Inductively Coupled Power Transfer Monorail Systems.* IEEE Transactions on Magnetics,, 2006. **42**(10): p. 3389-3391.
39. Gyu Bum, J. and B.H. Cho, *An energy transmission system for an artificial heart using leakage inductance compensation of transcutaneous transformer.* Power Electronics, IEEE Transactions on, 1998. **13**(6): p. 1013-1022.

40. Chwei-Sen, W., G.A. Covic, and O.H. Stielau, *Power transfer capability and bifurcation phenomena of loosely coupled inductive power transfer systems.* IEEE Transactions on Industrial Electronics, , 2004. **51**(1): p. 148-157.
41. Chwei-Sen, W., O.H. Stielau, and G.A. Covic, *Design considerations for a contactless electric vehicle battery charger.* IEEE Transactions on Industrial Electronics, , 2005. **52**(5): p. 1308-1314.
42 Covic, G.A. and J.T. Boys, *Modern Trends in Inductive Power Transfer for Transportation Applications.* IEEE Journal of Emerging and Selected Topics in Power Electronics, , 2013. **1**(1): p. 28-41.
43. Huh, J., et al., *Narrow-Width Inductive Power Transfer System for Online Electrical Vehicles.* IEEE Transactions on Power Electronics, , 2011. **26**(12): p. 3666-3679.
44. Kissin, M.L.G., J.T. Boys, and G.A. Covic, *Interphase Mutual Inductance in Polyphase Inductive Power Transfer Systems.* IEEE Transactions on Industrial Electronics, , 2009. **56**(7): p. 2393-2400.
45. Chen, Q., et al., *Analysis, Design, and Control of a Transcutaneous Power Regulator for Artificial Hearts.* IEEE Transactions on Biomedical Circuits and Systems, , 2009. **3**(1): p. 23-31.
46. Pinuela, M., et al., *Maximizing DC-to-Load Efficiency for Inductive Power Transfer.* IEEE Transactions on Power Electronics, , 2013. **28**(5): p. 2437- 2447.
47. Zhang, W., et al., *Analysis and Comparison of Secondary Series- and Parallel-Compensated Inductive Power Transfer Systems Operating for Optimal Efficiency and Load-Independent Voltage-Transfer Ratio.* IEEE Transactions on Power Electronics,, 2014. **29**(6): p. 2979-2990.
48. Steigerwald, R.L., *A comparison of half-bridge resonant converter topologies.* IEEE Transactions on Power Electronics,, 1988. **3**(2): p. 174-182.
49. Pantic, Z., B. Sanzhong, and S. Lukic, *ZCS LCC-Compensated Resonant Inverter for Inductive-Power-Transfer Application.* IEEE Transactions on Industrial Electronics, , 2011. **58**(8): p. 3500-3510.
50. Covic, G.A., et al., *A Three-Phase Inductive Power Transfer System for Roadway-Powered Vehicles.* IEEE Transactions on Industrial Electronics,, 2007. **54**(6): p. 3370-3378.
51. Zhang, W., et al., *Design for Efficiency Optimization and Voltage Controllability of Series-Series Compensated Inductive Power Transfer Systems.* IEEE Transactions on Power Electronics, , 2014. **29**(1): p. 191-200.
52. Hou, J., et al., *Precise Characteristics Analysis of Series/Series-Parallel Compensated Contactless Resonant Converter.* IEEE Journal of Emerging and Selected Topics in Power Electronics, , 2014. **PP**(99): p. 1-1.
53. Sallan, J., et al., *Optimal Design of ICPT Systems Applied to Electric Vehicle Battery Charge.* IEEE Transactions on Industrial Electronics, , 2009. **56**(6): p. 2140-2149.
54. Qu, X., et al., *Design of a Current-Source-Output Inductive Power Transfer LED Lighting System.* IEEE Journal of Emerging and Selected Topics in Power Electronics,, 2014. **PP**(99): p. 1-1.
55. Li S., et al., *A Double-Sided LCC Compensation Network and Its Tuning Method for Wireless Power Transfer*. IEEE Transactions on Vehicular Technology, , vol. PP, pp. 1-1, 2014.
56. Yilmaz, M. and P.T. Krein, *Review of Battery Charger Topologies, Charging Power Levels, and Infrastructure for Plug-In Electric and Hybrid Vehicles.* IEEE Transactions on Power Electronics, , 2013. **28**(5): p. 2151-2169.